Physics of the Earth and Planetary Interiors 222 (2013) 1–7

Contents lists available at SciVerse ScienceDirect

Physics of the Earth and Planetary Interiors

journal homepage: www.elsevier.com/locate/pepi

Effect of dynamic melting on acoustic velocities in a partially molten peridotite ☆

Li Li *, Donald J. Weidner

Mineral Physics Institute, Department of Geosciences, Stony Brook University, Stony Brook, NY 11794-2100, USA

ARTICLE INFO

Article history:
Received 24 January 2013
Received in revised form 15 June 2013
Accepted 21 June 2013
Available online 2 July 2013
Edited by M. Jellinek

Keywords:
Low velocity zone
Partial melting
Acoustic velocity

ABSTRACT

The mechanical effect of materials with a zero shear modulus aggregated with solids with non-zero shear moduli has been the primary motivation for why partially molten rocks should have lowered shear wave velocities. We propose that elastic softening associated with the process of melting must also be considered. In this view, seismic waves, propagating in regions of partial melting, perturb the thermodynamic state and drive solid to liquid and liquid to solid, thereby lowering the effective elastic moduli. We present measurements of Young's modulus for a mantle peridotite, KLB1, at LVZ pressures and temperatures and seismic frequency that support this model. The model predicts that the softening of elastic modulus is controlled by the pressure dependence of melt fraction, $\partial F/\partial P$, and not the percentage of melt present. In contrast to previous models, the P-wave velocity is decreased by nearly the same percentage as the S-wave velocity.

1. Introduction

The Earth's low velocity zone, ubiquitous in the shallow oceanic mantle, is associated with the base of the lithosphere. While partial melting has often been viewed as the cause of the lowered velocity (Anderson and Sammis, 1970; Harmon et al., 2009; Yang et al., 2007), detailed analysis indicates that the effect on velocity may be too small (Faul et al., 2004; Gribb and Cooper, 2000; Jackson et al., 2004).

In the center of the debate as to whether or not partial melting contributes to the low velocity zone, is the question of how do melts and melting affect the sound velocity. Melts lower the seismic velocity since liquid has a zero shear modulus and a composite of liquid inclusion and solid matrix produces an intermediate shear modulus. In this case, the shape of the liquid inclusions and volume fraction of melt dictate the softening effect (Anderson and Spetzler, 1970). The inadequacy of these models to sufficiently lower the shear velocity for a texturally equilibrated system and provide a seismic discontinuity with small amounts of melt challenges the association of low velocity zone and melting. The dynamics of the melting phase transformation offers a possible mechanism that can produce the seismic features of the low velocity zone with very little melt present.

Here we will describe the dynamic melting model and provide experimental data that support this view. In the dynamic melting model, the propagating elastic wave is viewed as a time dependent stress field that alters the thermodynamic state of the medium, and in regions of partial melting, will promote a small amount of crystallization or melting depending on the change in stress from the ambient values. The associated volume change introduces a strain in the medium and ultimately lowers the elastic modulus which is the ratio of stress to strain. The lowered elastic modulus results in a reduced acoustic velocity. O'Connell (1976) considered the role of volume changing phase transformations on postglacial rebound. The stress field of the melted ice sheet promotes a change in depth of the mantle phase transitions and leads to a contribution to the uplift. Anderson (1989) and Jackson (2007) discuss the role of volume changing phase transformations on attenuation of elastic waves. These discussions focus on the bulk modulus and emphasize the role of time scale on the process.

The inherent time scale of the volume changing process is defined by the kinetics of the transformation, the rheology of the medium, diffusion rates for various cations or a combination of all of these. Processes that are very fast compared to the period of the elastic wave will produce a 'relaxed' elastic modulus for the elastic wave with little attenuation while processes that are very slow compared to the period of the elastic wave will produce an 'unrelaxed' elastic modulus again with little attenuation. When the time scales of the process and the period of the elastic wave are comparable, then the elastic modulus is frequency dependent and the acoustic wave experiences maximum attenuation. In the case at hand, the time scales will be distributed over a wide band. The

* Corresponding author. Tel.: +1 631 632 6152.
E-mail address: lilli@ic.sunysb.edu (L. Li).

0031-9201/$ - see front matter © 2013 The Authors. Published by Elsevier B.V. All rights reserved.
http://dx.doi.org/10.1016/j.pepi.2013.06.009

important input will be how the volume change is distributed in time. Melting is a rather fast thermodynamic process. We anticipate that 80% of the melting occurs on very short time scale, while complete thermodynamic equilibrium may take millions of years. Li and Weidner (2008) and Ricard et al. (2009) emphasize the role of volume changing phase transformations in the transition zone in altering seismic velocity. Ricard et al. (2009) model the effect of volume-changing transitions on both the bulk modulus and the shear modulus. Shear modulus is affected, as described below, because of the local thermodynamic equilibrium conditions.

2. The dynamic melting model

The propagation of stress waves in fluid-bearing rocks have been studied both experimentally and theoretically for decades (Anderson and Sammis, 1970; Jackson et al., 2004; Mavko et al., 1979; Mavko and Nur, 1979; O'Connell and Budiansky, 1977). Models have been established to describe the effect of fluid on the velocity and attenuation of rocks. These models focus on descriptions of pore geometry and fluid distribution in defining different regimes such as drained, saturated isobaric and saturated isolated (O'Connell and Budiansky, 1977); where fluid can flow out of the bulk; can communicate between pores; and cannot communicate between pores respectively. A few mechanisms such as regional flow (Mavko and Nur, 1975), viscous (shear) relaxation (Walsh, 1969), stress-induced flow (O'Connell and Budiansky, 1977) or melt-squirt (Mavko and Nur, 1975) were proposed to describe the dynamic of fluid under stress waves. In regional flow models, the pore pressure of melt drives the flow of melts on kilometer length scale. Its relaxation time is defined by the liquid diffusion time (Nur and Booker, 1972) and is on 10^3 year time scale. In viscous relaxation models, relaxation of shear stresses is caused by the viscous shear flow of thin flat fluids parallel to the plane of the crack. Its relaxation time is on 10^{-2} to 10^3 second time scale. In stress-induced flow models, fluids flow between cracks with different orientations. Its relaxation time is on 3–5 year time scale. Depending on the variation of the relaxation time scale, these mechanisms have been used to explain seismic and post-seismic relaxation.

The common ground of these models is that the fluid and solid do not interact with each other. The difference among various models can be identified by the relaxation time and the difference of the effect on P *vs.* S wave velocity (or the shear *vs.* bulk component). For the viscous relaxation model, whose relaxation time is closest to the seismic wave period, the study (Walsh, 1969) reported similar effective bulk modulus between the composite and the solid, but the effective shear modulus is much lower for the composite. It coincides with the fact that if the effective modulus is an aggregate modulus between a solid modulus and a liquid modulus, the shear modulus is affected larger than the bulk modulus, since liquid has a drastically lower shear modulus than its solid form, while bulk modulus is not far different from that of the solid. We point out below that these models have not successfully predicted experimental studies which have used samples containing liquid–solid interacting such as peridotite and its melts (Sato et al., 1989) and water-brine (Spetzler and Anderson, 1968) as described below.

Here we express the elastic modulus as: $1/M = \varepsilon\sigma$, corresponding to stress boundary conditions, where M is either K, bulk modulus, or G, shear modulus, ε is strain and σ represents stress. The strain consists of the total elastic strain resulting from σ plus the strain caused by the volume changing phase transformation. In the case of bulk modulus, $\sigma = \delta P$ and $\varepsilon = \delta V/V$, with $\delta V/V = \delta P/K + (\delta V_{\text{transformation}}/V)$ where $\delta V_{\text{transformation}}$ is the volume change of the system due to the transformation that is driven by δP. In turn, $(\delta V_{\text{transformation}}/V) = (\delta P)\partial F/\partial P(V_{\text{liquid}} - V_{\text{solid}})/V$. Hence,

$$1/K_{\text{eff}} = 1/K_{\text{elas}} - (\partial F/\partial P)_S(V_{\text{liquid}} - V_{\text{solid}})/V \quad (1)$$

where K_{elas} is the elastic bulk modulus of the rock-melt aggregate; F is the volume fraction of melt; $\partial F/\partial P$ is the melt productivity and the subscript, S, indicates the adiabatic derivative; V is the aggregate volume. $(\Delta V/V)_{\text{melting}}$ is defined by the thermodynamics of the system and is independent of δP. The second term on the right reflects the volume strain introduced by the melting process. K_{eff} is the relaxed modulus.

To define the shear modulus, we must define the effect of shear stress on melting. To this end, we explore the effect in the principal-stress coordinate system, where the perturbation in stress from hydrostatic is simply expressed in a variation of the normal stresses from the hydrostatic. In his treatise on thermodynamics, Gibbs (1878) considered a case where a solid grain is bounded by 4 liquid reservoirs as illustrated in Fig. 1. The liquid reservoirs are mechanically isolated from each other but in mechanical contact with the solid. Thus, the normal stress in the solid at the solid–liquid interface is equal to the pressure in the adjacent liquid reservoir. Assuming that the third dimension has a normal stress of $\frac{1}{2}(P_1 + P_2)$, with no shear stresses in this coordinate system, then the stress state of the solid can be characterized by a pressure $P = \frac{1}{2}(P_1 + P_2)$ plus a shear stress of $\frac{1}{2}(P_1 - P_2)$ acting on the x_1–x_2 plane. The effective shear modulus, Γ_{eff}, will be $(P_1 - P_2)/(\varepsilon_1 - \varepsilon_2)$ where ε_1 is the longitudinal strain in the x_1 direction. Gibbs concluded that (1) this system is governed by local equilibrium. That is, the equilibrium between the solid and the liquid at the liquid 1 interface is as though the system were at the pressure, P_1, and the equilibrium at the liquid 2 interface is as though the system were at the pressure, P_2. He further concluded that (2) the Gibbs free energy is not a state function in this system, since the equilibrium is governed by the local orientation of interfaces. The consequences of this first conclusion is that for a solid-melt that has equilibrated at pressure, P, and then subjected to a shear stress, will experience increased melting on interfaces of reduced normal stresses and solidification on interfaces of increased normal stresses. The consequence of the second conclusion is that the actual amount of melting and solidification can only be specified if the geometry of all interfaces is specified. Thus, while it is necessary that thermodynamic induced melting and solidification are expected to accommodate shear waves, the amount of shear modulus softening is not uniquely defined. If we assumed that: $\varepsilon_1 = \varepsilon_{1\text{elastic}} + \Delta V/V$, where $\Delta V/V$ is the volume change associated with a

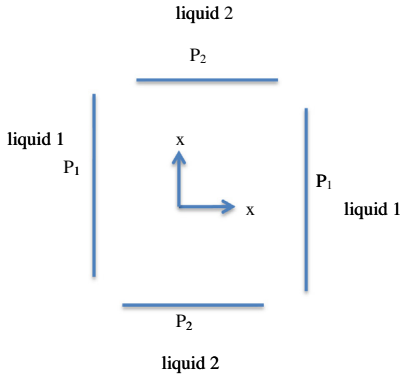

Fig. 1. Illustration of a solid under both thermodynamic and mechanical equilibrium with four liquid reservoir, adapted from Gibbs (1878). In the solid, $\sigma_1 = P_1$ and $\sigma_2 = P_2$ yielding a shear stress of $\frac{1}{2}(P_1 - P_2)$ on the x_1–x_2 plane. The liquid reservoir can be smaller than the thickness of the line in the system. The equilibrium is defined on a local scale and governed by the normal stress in the solid–liquid interface. Thus, a shear stress will promote solidification on one reservoir and melting on the other with no net change in the total melt fraction. However, a modulus-softening shear strain will result.

pressure change of ½($P_1 - P_2$) normalized to the volume of the system then

$$1/G_{\text{eff}} = 1/G_{\text{elas}} - (\partial F/\partial P)_T(V_{\text{liquid}} - V_{\text{solid}})/V \quad (2)$$

This effect is independent of the amount of fluid in the reservoir, to the point where the grains on opposite sides of the reservoir may actually touch, as long as the grains are in equilibrium with the partial melt. Thus, we see that the reduction in both the bulk modulus and the shear modulus depends on the melt productivity ($\partial F/\partial P$) and does not depend on either the amount of melt present or on the magnitude of pressure perturbation, δP.

The effect of a volume changing transformation on the shear modulus was modeled for the olivine–wadsleyite transformation (Ricard et al., 2009) using a spherical grain model with relaxation times arising from the kinetics of the phase transformation. The authors conclude that the shear modulus is relatively more decreased than the bulk modulus for all time scales and that the relaxed, thermodynamically equilibrated shear modulus is zero.

The model proposed here has similarities to the melt squirt model in that pockets of fluid that experience an increase in pressure will have fluid in the cavity diminish and fluid in cavities with lowered pressure will have fluid volume increase. A major difference is that for the dynamic melt model, regions with no fluid present will have fluid increase as pressure is diminished (solids will melt even if no fluid is present as long as the chemistry is present). Thus, the magnitude of the effect of melting will be larger than the melt-squirt model would predict. Furthermore, no plumbing system is required for the melting model to transport fluid from one cavity to another. In addition, the melt-squirt model has no effect on the bulk modulus where pressure is increased uniformly in all cavities.

3. Experimental data

3.1. Previous data

There have been two classic experimental studies that measure elastic properties ultrasonically during the melting process (Sato et al., 1989; Spetzler and Anderson, 1968). These have been widely used as constrains for the solid–liquid aggregate models for representing partial melting. Aggregate models typically define shear modulus as a function of small amounts of liquid and the geometric distribution of the liquid. The models predict virtually no change in the bulk modulus under these conditions.

Spetzler and Anderson (1968) studied a salt-water mixture that produced a binary melting relation. They report data for two compositions, one with 1% NaCl and the other with 2% NaCl, yielding a factor of two in the amounts of melt at any temperature within the partial melting zone. They found that upon the initial melting at the eutectic of the lower NaCl system with formation of 3% liquid, the shear modulus dropped by about 25% and the bulk modulus dropped by 8%. The higher NaCl system, with 6% melt experienced a decrease in bulk modulus of over 30% with more than 60% decrease for shear modulus. Furthermore, at the temperature with 6% melt in the low salt system, the bulk modulus decrease was about 1/3 and the shear modulus decrease was 1/2 of that for the high salt system with 6% melt. In retrospect, these results challenge the standard mechanical model for partial melting in two respects. (1) The bulk modulus should not decrease this much for such a small amount of melt. (2) The elastic moduli should be dominated by the fraction of melt present since the melt geometry was similar for the two systems. The dynamic melting model is compatible with both of these observations as both the bulk modulus and the shear modulus will decrease with melting, and $\partial F/\partial P$, not F, dictates the amount of decrease.

The second study was for partial melting of a peridotite (Sato et al., 1989). A substantial drop in sound velocities occurred with the onset of melting. But, again, the relative drop in P velocity was equal to the relative drop in shear velocity, which yields a value for d($ln(Vs)$)/d($ln(Vp)$) of 1.0. For a peridotite with only the shear modulus decreasing, the value of d($ln(Vs)$)/d($ln(Vp)$) would be 2.3. Our model, including the adiabatic effect for bulk modulus, yields a value of d($ln(Vs)$)/d($ln(Vp)$) of 1 in agreement with these experiments. Our conclusion is that the laboratory data from ultrasonic studies support the dynamic melting model and is incompatible with a two-phase aggregate model. Going one step further, this leads us to conclude that the kinetic time of melting is probably very fast, on a microsecond time scale.

Recent studies of the low frequency shear modulus for a system of olivine plus basalt melt (Jackson et al., 2004) indicated little or no effect of a few percent liquid. The dynamic melting model is also compatible with this since the value of $\partial F/\partial P$ is very small for this system once the basalt has melted.

3.2. Results for peridotite at mantle pressure

The experimental technique is described elsewhere (Li and Weidner, 2007, 2008, 2010; Weidner et al., 2010; Weidner and Li, 2007). The essence of the method is that the length of the sample and the accommodating stress proxy is measured as a function of time from X-ray radiograph. The exposure time of the X-ray image is 0.1 s. Images are taken every 10 deg of the sine wave. The sine wave is generated by the DDIA pumping system. The effective Young's modulus of the sample (E_{sample}) is derived from strains of the sample and proxy as $E_{\text{sample}} = E_{\text{proxy}} \times \varepsilon_{\text{proxy}}/\varepsilon_{\text{sample}}$, where the strain is the amplitude of the sine wave. Pressure is determined by the cell volume of olivine measured by X-ray diffraction and thermal equation of state of olivine (Isaak, 1992).

In these experiments, the sample is compressed to 1.5 GPa, annealed at 1273 K (subsolidus), then heated to above the solidus (1673 K). The effective Young's modulus is measured as pressure is increased by 0.6 GPa from the partial melt region to pressures where no liquid is present over a period of 15 h. Pressure was then increased by another 3 GPa at constant temperature in order to confirm that the increase in Young's modulus was not just pressure induced. Our goal is to define changes in elastic moduli due to melting as we cross the solidus. We choose to use pressure as our variable instead of temperature in order to avoid mixing the thermally activate effects with the melting effects (Jackson et al., 2002).

Over this pressure range including the solidus (0.6 GPa) the Young's modulus increases fourfold (Fig. 2a) attaining a value of about 200 GPa which is near the value expected for the dry peridotite. Each data point represents the effective elastic modulus derived from the magnitude of the sinusoidal strain during forced oscillation. The amplitude of the oscillating stress field is about 200 MPa. On further compression to 5 GPa confining pressure, the Young's modulus remained at this value. At the peak melting conditions, the volume of melt is expected to be less than 10%.

In order to compare the expected value with that observed, we calculate the magnitude of the relaxed Young's modulus from Eqs. (1) and (2) using a thermodynamic data base and the alphaMelts programs (Smith and Asimow, 2005). Fig. 2b illustrates the effect of melting on the Young's modulus for KLB1 for the same conditions as the experiments. Also illustrated here is the percent of partial melt. There is a strong increase in the Young's modulus over the pressure range where the melt is expected to vanish and the observed increase in modulus agrees with the model based on dynamic melting.

The recovered KLB1 sample was examined using scanning electron microscope. The sample from this run experienced a complex

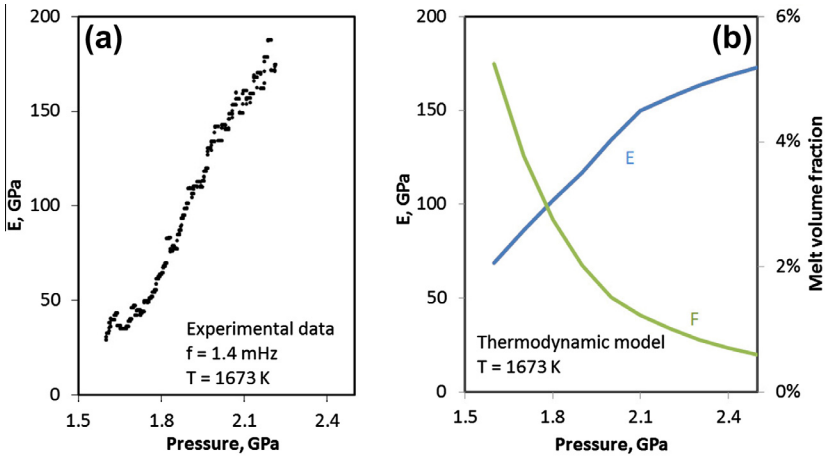

Fig. 2. Effective Young's modulus (E) of KLB1 peridotite as a function of pressure at 1673 K. Data in (a) are experimental results measured using synchrotron X-rays (Li and Weidner, 2008). Results in (b) are calculated using Eqs. (1)–(2) to illustrate the effect of dynamic melting on E. The variable dF/dP is derived from alphaMelts (Smith and Asimow, 2005) database. Also plotted in (b) is the melt volume fraction melt (F), which illustrates that melting is diminished by increasing pressure.

history that included cold compression to 1.5 GPa, annealing at 1273 K (subsolidus) for an hour, further heating to above the solidus (1673 K), forced oscillation for a period of 15 h at 1673 K as pressure range increased from 1.5 GPa to 2.3 GPa, and finally relatively rapid pressure increase to 5 GPa at 1673 K. The SEM image illustrated in Fig. 3 shows the recovered sample. The sample contains garnet, a phase that is stable at the highest pressure of this history. In this image, there are numerous apparent triple junctions present, which are probably relics of the partial melts. The sample remains homogeneous, indicating little mobility of melt and that the melt fraction is small.

4. Applicability of laboratory measurements to Earth

The above experiments were carried out at the pressure and temperature conditions of the Earth's low velocity zone using starting materials that come from a mantle rock at a frequency consistent with seismic frequencies. On the other hand the amplitude of the oscillating stress is larger than in a seismic wave, and the grain size of the laboratory sample is smaller than expected in the mantle. As a result, the measurements may be sampling non-linear elasto/plastic behavior or the time scale of the processes may be affected by the experimental procedure.

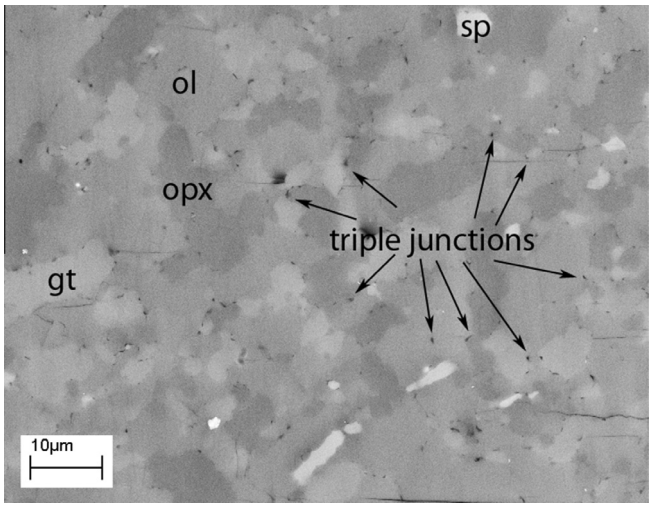

Fig. 3. Recovered sample quenched at 5 GPa and 1673 K from the in situ experiment as in Fig. 1. Ol, olivine; opx, orthopyroxene; gt, garnet, sp, spinel.

The observation of non-linear *vs.* linear attenuation has been associated with strain amplitude dependence (Mavko et al., 1979). Non-linear response is observed at strains larger than 10^{-6} and low effective confining pressures. However, materials containing no microcracks show no variation of amplitude dependence of attenuation (Winkler and Nur, 1979; Winkler et al., 1979). Studies carried out at high pressure (300 MPa) and strain (10^{-6}) (Jackson et al., 1992) did not show non-linear attenuation. Studies at mantle pressure (>5 GPa) (Li and Weidner, 2008) also showed a linear response for strain as large as 10^{-4}. It indicates that high pressure may suppress the strain amplitude dependence through minimizing pores and minicracks. Pressure also makes grain-boundary friction a less important energy loss. Still, non-linear processes will lower the elastic modulus below the elastic value. Since the observed high pressure value of the Young's modulus in this study agrees with the linear elastic value, we conclude that non-linear effects are not dominating the data.

In order for the phase transitions to soften elastic moduli, the kinetics of the transition should be faster than the sampling time of the measurement. Melting is one of the fastest phase transitions in silicates. Temperature quenching of peridotite melts at high pressure generally yields crystals, not glass. This suggests that the solidification process is fast compared to the 1 s quench time. However, Pertermann and Hirschmann (2003) indicate that several hours are required for complete thermodynamic equilibrium of the solid–liquid system at a fixed P, T. Thus, we expect some time distribution of the process towards equilibrium. The significant factor becomes how much volume change is associated with the different time scales. The answer to this question will define the frequency dependence of the elastic modulus and attenuation.

The kinetic rate of the transition can be controlled by (1) the velocity of the phase boundary and the distance that the phase boundary needs to move to achieve equilibrium, (2) the diffusion time for necessary atoms to reach their equilibrium distribution, or (3) the strength of the host solids to support pressure variations of the fluid filled voids. For the first case, the characteristic time is given by $\tau = x/v$ where x is the characteristic length and v is the velocity of the phase boundary. This process is often described by a velocity of the form:

$$v = AT \exp\left\{-\frac{\Delta H + PV^*}{RT}\right\}\left(1 - \exp\left\{\frac{-\Delta G}{RT}\right\}\right) \quad (3)$$

where A is a constant, T is temperature, ΔH is the activation enthalpy, P is pressure, V^* is the activation volume, and ΔG is the excess Gibbs free energy arising from the stress in the acoustic wave (Kubo et al., 2004; Turnbull, 1956). Since this latter quantity is quite small, we can replace the term in parenthesis by $\Delta G/RT$ or by $\Delta V\delta P/RT$ where ΔV is the volume change of the phase transition and δP is the excess pressure associated with the stress wave. Since all other values remain constant as the wave moves through the system, we have $v = B\delta P$, or simply, transformation rate, and hence velocity, is proportional to pressure perturbation. Jackson (2007), Li and Weidner (2008), and Ricard et al. (2009) show that the characteristic length, x, which is the width of the rim that is added to a grain of dimension, d is also proportional to δP. Thus, the characteristic time of this process is independent of the pressure perturbation. Thus, laboratory data are limited by the same time constraint as are acoustic data for this process.

For diffusion, the characteristic time is related to the characteristic length by $\tau = x^2/D$ where D is the diffusion coefficient. Here smaller stress perturbations will lower the characteristic time since x varies linearly with δP. Grain size will affect the kinetics since x will increase linearly with grain size. Thus, the characteristic time for diffusion will vary as $\tau = A\delta P^2 d^2$ where d is the grain size.

We can address the role of diffusion by examining the effect on $(\partial F/\partial P)$ of various perturbations of the system using the alphaMELTS program system. In melting phenomena, the chemical ingredients for the liquid are generally brought together at the grain boundaries, rendering solid-state diffusion as unnecessary. When three or more phases are present, only two phases will share a planer interface. The important issue then becomes how much of the melting will proceed if only two of the phases are in contact and the other phases are out of chemical communication. We address this issue by calculating $(\partial F/\partial P)$ with one of the phases chemically subtracted from the starting composition. This is meant to simulate melting at an interface on a short time when diffusion from that phase cannot affect the equilibrium. Fig. 4 illustrates several model calculations for melting as a function of pressure. Fig. 4a illustrates the volume fraction of melt present in the system, Fig. 4b shows the percent change in bulk modulus as a function of pressure, and Fig. 4c demonstrates the percent change in shear velocity. The isothermal curve corresponds to KLB1 at 1673 K. The no-opx curve represents the values for KLB1 with the orthopyroxene phase removed. Here the principle interaction is between olivine and clinopyroxene. This curve reflects dF/dP that would be formed if the orthopyroxene could not chemically communicate with the other two phases. We see very little difference in the

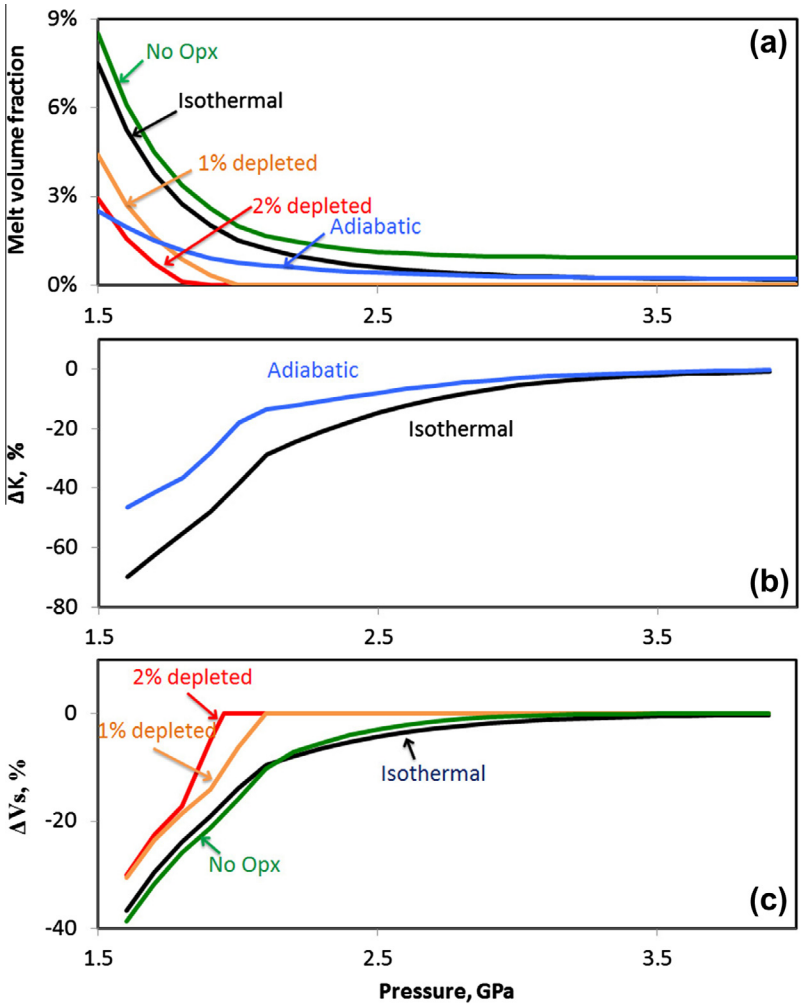

Fig. 4. The effect of dynamic melting on elastic properties. Panel (a) illustrates the melt volume fraction derived from alphaMelts (Smith and Asimow, 2005) database. Isothermal represents KLB1 at 1673 K; no Opx represents the KLB1 composition at 1673 K with orthopyroxene removed; 1% depleted represents the KLB1 composition at 1673 K with 1% of melt removed; likewise for 2% depleted; adiabatic represents the KLB1 composition with temperature varying along an isentrope. Panels (b) and (c) are calculated using Eqs. (1)–(2) to illustrate the effect of dynamic melting. Panel (b) illustrates the percent reduction of the bulk modulus. Panel (c) illustrates the percent reduction of the shear velocity.

effect on either the volume fraction of melt or on the shear modulus. Thus, phase boundary melting should be effective, even at short times, in reducing the elastic moduli.

Both experiments and calculations correspond to isothermal pressure variations. However, K is adiabatic in the acoustic wave; G is generally isothermal because both solidification and melting occur in a shear wave. Fig. 4b compares the calculated isothermal and adiabatic K. The effect of melting on the adiabatic K is about half as in the isothermal case for KLB1. Vp needs to be calculated using adiabatic K and isothermal G at the same temperature. Our calculated Vp shows that the percent softening is similar for Vp and Vs.

In all of these calculations, the effect of melting on the elastic properties depends on the melt productivity ($\partial F/\partial P$) and is independent of the amount of melt present. As further illustration, we simulate a depleted model in which 2% melt is removed from the initial composition. The resulting shear velocity reduction is illustrated in Fig. 4c. The curve is similar to the KLB1 curve in the region where melting exceeded 2%, but drops to zero at higher pressures where no melting is occurring. The same effect, but a lower amount of melting is demonstrated for the case with only 1% of melt removed.

The calculated thermodynamic models of Fig. 4 can be used to define the effect of partial melting in the oceanic upper mantle. The transition from partially molten to melt free can produce very smooth velocity profile as for the KLB1 model, or quite abrupt if some amount of melt has been extracted from the partially molten zone. The abrupt transition would produce a sharp seismic interface such as has been observed with body wave reflection analysis (Kawakatsu et al., 2009; Schmerr, 2012). The gradual transition could be more appropriate for the bottom of the low velocity zone.

In all of the above considerations, the fluid geometry plays a very substantial role in defining the effective elastic properties of the aggregate. The dynamic melting model needs fluids available to solidify under compression. Furthermore, the strength of the solid matrix can help buffer the pressure of the fluid from the stress perturbation of the seismic wave (Ricard et al., 2009). However, this is very sensitive to grain shape. Spherical melt pockets will be more effectively sheltered than pancake shaped pockets.

Melt geometry affects the total energy of the system by virtue of surface energies arising from interfaces. We expect that the melt distribution in the mantle will be close or at an equilibrium melt distribution, but that the response to a traveling seismic wave will be dominated by the chemical thermodynamics. The amount of melting during a seismic wave will be too small and the time will be too short for the distribution of melt to change. Thus, a complete model of dynamic melting will consider a hybrid of equilibrium and non-equilibrium melt structures.

The equilibrium geometry for small amounts of melt is dominated by triple junction tubes of fluid that interconnect into a matrix (Gribb and Cooper, 2000; Jackson et al., 2006; von Bargen and Waff, 1986; Zhu et al., 2011). This arises from the low wetting angle of the liquid–solid interface. This model needs to be tempered by TEM observation by de Kloe et al. (2000), Drury and Fitz Gerald (1996), Gribb and Cooper (2000)) that observe a thin film of melt on the grain interface in a partially melted peridotite, particularly for deforming samples. Furthermore, theoretical studies (Deymier et al., 1987; Tang et al., 2006) using molecular dynamics indicate that adjacent surfaces will promote melting between the surfaces at much lower temperatures than the melting point, suggesting that a thin liquid layer between two solids significantly lowers the surface energies of the system. This affect is probably enhanced by pressure. So a picture emerges with most of the fluid forming an interconnecting plumbing system with some fluid possibly in thin boundaries between grains. But this is not yet the equilibrium state as the interconnected system will drain as driven by gravity. The real Earth melt structure will be the final state created by partial melting, interactive plumbing system, and finally, by draining. The distribution of melt in this final state is even more complex to define.

5. Discussion

In order to explain the observed low velocity zone in the Earth (circa 10%) (Anderson and Spetzler, 1970), a few partial melting scenarios are possible. 6% melt in spherical pockets (Birch, 1969) causes enough softening on the aggregate elastic properties. 1% of melt with very small aspect ratios ($<10^{-3}$), concentrated at grain boundaries, also causes enough softening (Anderson and Spetzler, 1970). As shown by Fig. 4c, dynamic melting causes the required softening with less than 2% melts for the KLB1 model. For both the 1% depleted and 2% depleted model, the required amount of melt is less than 1% for Vs to decrease 10%. We conclude that, for small amounts of melt, the softening effect caused by dynamic melting dominates the effect of melts for spherical inclusions and is competitive with the effect of melts for inclusions with high aspect ratios.

Eq. (1) is straightforward for defining the relaxed bulk modulus for a partially molten system. The effect of melting on the shear modulus is governed by local processes and is thereby more complex. For example, if the material has attained a state where the liquid is localized in isolated tubes, then the compression cycle of the stress wave may not be able to solidify any of the liquid. However, since the solid is in equilibrium with a liquid, the dilatational phase of the stress wave should produce melting at interfaces between two of the fertile minerals, such as olivine and clinopyroxene as illustrated above. Thus, the melting induced strain during a full cycle should be at least half of the strain estimated in Eq. (2).

The phenomena illustrated here are inescapable for any region in the Earth at temperatures above the solidus. Indeed, the low velocity zone is expected to be a region where melts are coexisting with the solid matrix, particularly considering the role of water and CO_2 in lowering the temperature of the solidus (Hirschmann, 2010; Karato, 2012). The primary assumption in applying the models in Fig. 4 to the Earth is that the time scale of the measurement is long compared to the time scale for volume-changing melting. Surface waves with periods between 100 and 500 s are the primary evidence for the upper mantle low velocity zones. We assert that stress induced melting must contribute to the lowering of the shear modulus if partial melting is present.

Acknowledgments

We wish to thank Michael Vaughan for support for this project. Ian Jackson provided critical input that helped the manuscript. This research was partially supported by COMPRES, the Consortium for Materials Properties Research in Earth Sciences under NSF Cooperative Agreement EAR 10-43050. Support from the NSLS by the U.S. DoE, under Contract No. DE-AC02_98CH10886. The authors acknowledge support by the NSF EAR1141895, EAR1045629, and EAR0968823.

References

Anderson, D.L., 1989. Theory of the Earth. Blackwell Scientific Publications.
Anderson, D.L., Sammis, C.G., 1970. Partial melting in the upper mantle. Phys. Earth Planet. Inter. 3, 41–50.
Anderson, D.L., Spetzler, H., 1970. Partial melting and the low-velocity zone. Phys. Earth Planet. Inter. 4, 62–64.
Birch, F., 1969. Density and composition of the upper mantle: first approximation as an olivine layer. In: The Earth's Crust and Upper Mantle, Geophys. Monograph 13. American Geophysical Union, Washington, DC, pp. 18–36.

de Kloe, R., Drury, M.R., vanRoermund, H.L.M., 2000. Evidence for stable grain boundary melt films in experimentally deformed olivine–orthopyroxene rocks. Phys. Chem. Minerals 27, 480–494.
Deymier, P., Taiwo, A., Kalonji, G., 1987. A grain-boundary phase-transition studied by molecular-dynamics. Acta Metall. 35, 2719–2730.
Drury, M.R., Fitz Gerald, J.D., 1996. Grain boundary melt films in an experimentally deformed olivine–orthopyroxene rock: implications for melt distribution in upper mantle rocks. Geophys. Res. Lett. 23, 701–704.
Faul, U.H., Gerald, J.D.F., Jackson, I., 2004. Shear wave attenuation and dispersion in melt-bearing olivine polycrystals: 2. Microstructural interpretation and seismological implications. J. Geophys. Res.: Solid Earth 109, B06202. http://dx.doi.org/10.1029/2003JB002407.
Gibbs, J.W., 1878. Equilibrium of heterogeneous substances. Trans. Connecticut Acad. 3, 343–524.
Gribb, T.T., Cooper, R.F., 2000. The effect of an equilibrated melt phase on the shear creep and attenuation behavior of polycrystalline olivine. Geophys. Res. Lett. 27, 2341–2344.
Harmon, N., Forsyth, D.W., Weeraratne, D.S., 2009. Thickening of young Pacific lithosphere from high-resolution Rayleigh wave tomography: a test of the conductive cooling model. Earth Planet. Sci. Lett. 278, 96–106.
Hirschmann, M.M., 2010. Partial melt in the oceanic low velocity zone. Phys. Earth Planet. Inter. 179, 60–71.
Isaak, D.G., 1992. High-temperature elasticity of iron-bearing olivines. J. Geophys. Res.: Solid Earth 97, 1871–1885.
Jackson, I., 2007. Physical origins of anelasticity & attenuation in rock. In: Schubert, G. (Ed.), Treatise on Geophysics. Elsevier, Amsterdam.
Jackson, I., Faul, U.H., Fitz Gerald, J.D., Morris, S.J.S., 2006. Contrasting viscoelastic behavior of melt-free and melt-bearing olivine: implications for the nature of grain-boundary sliding. Mater. Sci. Eng., A 442, 170–174.
Jackson, I., Faul, U.H., Fitz Gerald, J.D., Tan, B.H., 2004. Shear wave attenuation and dispersion in melt-bearing olivine polycrystals: 1. Specimen fabrication and mechanical testing. J. Geophys. Res.: Solid Earth 109, B06201. http://dx.doi.org/10.1029/2003JB002406.
Jackson, I., Fitz Gerald, J.D., Faul, U.H., Tan, B.H., 2002. Grain-size-sensitive seismic wave attenuation in polycrystalline olivine. J. Geophys. Res.: Solid Earth 107 (B12), 2360. http://dx.doi.org/10.1029/2001JB001225.
Jackson, I., Paterson, M.S., Fitz Gerald, J.D., 1992. Seismic-wave dispersion and attenuation in Aheim dunite – an experimental-study. Geophys. J. Int. 108, 517.
Karato, S.I., 2012. On the origin of the asthenosphere. Earth Planet. Sci. Lett. 321, 95–103.
Kawakatsu, H., Kumar, P., Takei, Y., Shinohara, M., Kanazawa, T., Araki, E., Suyehiro, K., 2009. Seismic evidence for sharp lithosphere–asthenosphere boundaries of oceanic plates. Science 324, 499–502.
Kubo, T., Ohtani, E., Funakoshi, K.-I., 2004. Nucleation and growth kinetics of the {alpha}-{beta} transformation in Mg_2SiO_4 determined by in situ synchrotron powder X-ray diffraction. Am. Mineral. 89, 285–293.
Li, L., Weidner, D., 2008. Effect of phase transitions on compressional-wave velocities in the Earth's mantle. Nature 454, 984.
Li, L., Weidner, D., 2010. Synchronized stress–strain measurements in dynamic loading at high pressure using D-DIA. Rev. Sci. Instrum. 81, 096102. http://dx.doi.org/10.1063/1.3481163.
Li, L., Weidner, D.J., 2007. Energy dissipation of materials at high pressure and high temperature. Rev. Sci. Instrum. 78. http://dx.doi.org/10.1063/1061.2735587.
Mavko, G., Kjartansson, E., Winkler, K., 1979. Seismic-wave attenuation in rocks. Rev. Geophys. 17, 1155–1164.
Mavko, G., Nur, A., 1975. Melt squirt in asthenosphere. J. Geophys. Res. 80, 1444–1448.
Mavko, G.M., Nur, A., 1979. Wave attenuation in partially saturated rocks. Geophysics 44, 161–178.
Nur, A., Booker, J.R., 1972. Aftershocks caused by pore fluid-flow. Science 175, 885.
O'Connell, R.J., 1976. The effects of mantle phase changes on postglacial rebound. J. Geophys. Res. 81, 971–974.
O'Connell, R.J., Budiansky, B., 1977. Viscoelastic properties of fluid-saturated cracked solids. J. Geophys. Res. 82, 5719–5735.
Pertermann, M., Hirschmann, M.M., 2003. Anhydrous partial melting experiments on MORB-like eclogite: phase relations, phase compositions and mineral–melt partitioning of major elements at 2–3 GPa. J. Petrol. 44, 2173–2201.
Ricard, Y., Matas, J., Chambat, F., 2009. Seismic attenuation in a phase change coexistence loop. Phys. Earth Planet. Inter. 176, 124–131.
Sato, H., Sacks, I.S., Murase, T., 1989. The use of laboratory velocity data for estimating temperature and partial melt fraction in the low-velocity zone – comparison with heat-flow and electrical-conductivity studies. J. Geophys. Res.: Solid Earth 94, 5689–5704.
Schmerr, N., 2012. The Gutenberg discontinuity: melt at the lithosphere–asthenosphere boundary. Science 335, 1480–1483.
Smith, P.M., Asimow, P.D., 2005. Adiabat_1ph: a new public front-end to the MELTS, pMELTS, and pHMELTS models. Geochem. Geophys. Geosyst. 6 (1), 2004GC000816. ISSN 1525-2027.
Spetzler, H., Anderson, D.L., 1968. Effect of temperature and partial melting on velocity and attenuation in a simple binary system. J. Geophys. Res. 73, 6051–6060.
Tang, M., Carter, W.C., Cannon, R.M., 2006. Grain boundary order–disorder transitions. J. Mater. Sci. 41, 7691–7695.
Turnbull, D., 1956. Phase changes. In: Seitz, F., Turnbull, D. (Eds.), Solid State Physics, David Turnbull, pp. 225–306.
von Bargen, N., Waff, H.S., 1986. Permeabilities, interfacial-areas and curvatures of partially molten systems – results of numerical computation of equilibrium microstructures. J. Geophys. Res.: Solid Earth 91, 9261–9276.
Walsh, J.B., 1969. New analysis of attenuation in partially melted rock. J. Geophys. Res. 74, 4333.
Weidner, D.J., Vaughan, M.T., Wang, L., Long, H., Li, L., Dixon, N., Durham, W.B., 2010. Precise stress measurements with white synchrotron X-rays. Rev. Sci. Instrum. 81, 013903.
Weidner, D.J., Li, L., 2007. Method for the study of high P/T deformation and rheology. In: Schubert, G. (Ed.), Treatise on Geophysics. Mineral Physics: Theory and Practice. Elsevier.
Winkler, K., Nur, A., 1979. Pore fluids and seismic attenuation in rocks. Geophys. Res. Lett. 6, 1–4.
Winkler, K., Nur, A., Gladwin, M., 1979. Friction and seismic attenuation in rocks. Nature 277, 528–531.
Yang, Y.J., Forsyth, D.W., Weeraratne, D.S., 2007. Seismic attenuation near the East Pacific Rise and the origin of the low-velocity zone. Earth Planet. Sci. Lett. 258, 260–268.
Zhu, W.L., Gaetani, G.A., Fusseis, F., Montesi, L.G.J., De Carlo, F., 2011. Microtomography of partially molten rocks: three-dimensional melt distribution in mantle peridotite. Science 332, 88–91.